Proceedings of the 26th International Conference on
Port and Ocean Engineering under Arctic Conditions
June 14-18, 2021, Moscow, Russia

Influence of the Constraint Force Mixing Parameter in Non-smooth DEM Simulation on Global Ice Load by Managed Ice Floes

Kenta Hasegawa [1], Takatoshi Matsuzawa [1]
[1] National Maritime Research Institute, National Institute of Maritime, Port and Aviation Technology, Tokyo, Japan

ABSTRACT

This paper has presented the results of three-dimensional non-smooth discrete element simulations for a structure-multiple ice floes interaction under managed ice conditions. To represent ice failure, the authors introduced a breakable ice element consisting of small square rigid bodies with a fixed joint function of the physics engine of Bullet to our simulation model. Bullet physics engine uses parameters of the constraint force mixing (Σ) and the error reduction parameter to permit Baumgarte stabilization method which reduces constraint error efficiently. Since it is reported that Σ greatly contributes to the hardness of constraints, we performed the plate deflection test in the numerical simulation and compare with the experiment data. The primary finding is that an elastic modulus of an ice floe can be determined by the element size and the constraint force mixing parameter. To investigate the effect of the elastic modulus determined by this approach on ice load, numerical simulations were conducted under managed ice conditions using 0.6 m-square ice floes with the ice elastic modulus of about 200, 60, and 30 MPa, respectively. The simulated result for the ice floes with an elastic modulus of 200 MPa indicates the smaller mean ice load and the larger number of broken ice floes compared to that with an elastic modulus of 60 MPa. This can be explained based on the hybrid model using Lindqvist and KPR models.

KEY WORDS: Non-smooth Discrete Element Method; Constraint Force Mixing; Baumgarte stabilization method; Managed Ice Floes; Global Ice Load Ice.

INTRODUCTION

The United States Geological Survey has reported that about 13% of the world’s undiscovered oil and 30% of the world’s undiscovered gas may be found in the area north of the Arctic Circle (Gautier and Moore, 2017). It is also mentioned that sea ice has been declining in the Arctic sea, where oil and gas development is expected. Arctic resource development, however, suffers great threat from sea ice and iceberg. In the case of using a floating structure such as a drilling rig at sites where sea ice exists, ice management which is an operation to break sea ice into smaller pieces by icebreakers is carried out in order to reduce the ice load and improve the station keeping ability.

Managed ice floes collide with the structure or other floes resulting in horizontal and/or vertical displacement and in some cases global ice failure such as bending or splitting occurs. To numerically simulate such managed ice floes-structure interaction, it is necessary to deal with multiple body problems. Discrete Element Methods (DEMs) are often used for these problems in many fields. In ice engineering, for example, Polojärvi et al. (2012) have conducted and simulated laboratory-scale punch through tests on floating rubble consisting of plastic blocks with a 3D discrete numerical model. Konno et al. (2013) have numerically reproduced brash ice channel experiments with more than 10^4 ice pieces by using the Open Dynamics Engine (ODE). Lubbad and Løset (2015) have developed a simulator dealing with the interaction between managed ice and floating structures by DEM with analytical closed form solutions to represent the icebreaking processes. However, there is little literature comparing ice loads, the behavior of ice floes, and ice failure between numerical simulations and ice tank tests on managed ice conditions. The authors have been developing a DEM simulation by using the Bullet Physics (Coumans, 2017), one of the open source dynamics libraries, since 2017 and showed some results such as the size effect of ice floes and the overestimated peak load measured in an ice tank test conducted in 2017 at the ice model basin of National Maritime Research Institute (Hasegawa et al., 2018; 2019a). In this simulation, ice failure, which was observed in the test, was not taken into account. Hasegawa et al. (2019b) introduced a breakable ice element consisting of small rigid bodies with a fixed joint function of the physics engine to our numerical simulation method in order to represent ice failure. The results show that the breakable ice elements reasonably reduce peak loads to the experiment.

Bullet physics engine uses parameters of the constraint force mixing (Σ) and the error reduction parameter when adopting the fixed joint function to permit Baumgarte stabilization method which reduces constraint error efficiently. Σ can be expressed by a time step, spring and damping constants, and Smith (2006) has reported that Σ greatly contributes to the hardness of constraints. In this study, therefore, we investigated the relationship between the elastic modulus of the ice model and constraint stabilization parameters used in the physics engine when combining ice elements.

NUMERICAL SIMULATION

Non-smooth Discrete Element Method

Discrete Element Methods (DEMs) are often used for multiple body problems in many fields. There are roughly two approaches in DEMs, one is a smooth approach (Cundall and Strack, 1979) in which an interaction force is applied according to the penetration amount of objects by taking into account of the viscoelasticity nature of contact. The other is a non-smooth approach (Jean, 1999) in which objects are assumed to be rigid in general. Collision and stick-slip friction transition are considered as instantaneous events according to the given contact law. The authors compared the results by non-smooth DEM simulation with the experimental results in the case of single ice floe-structure interaction and showed that the impact load can be qualitatively reproduced well (Hasegawa et al., 2018). The projected Gauss-Seidel method (Catto, 2005) is used for solving the constraint forces by satisfying the constraint condition at each time step. To implement the non-smooth DEM, Bullet Physics Library version 8.26 developed by Coumans (2017) was used in this study.

Breakable Ice Element

The image of the breakable ice element adopted in this paper is shown in Figure 1. An ice floe is divided into small rigid elements which are connected to each other through a fixed joint function of the physics engine. Ice failure is simply represented by disconnecting the joint when the constraint force exerted on the joint exceeds a threshold based on ice strength. This approach is often used for a collapse simulation of a building which is necessary to track a large number of fragments, e.g., in Hamano et al. (2016) and in Walter and Kostack (2015).

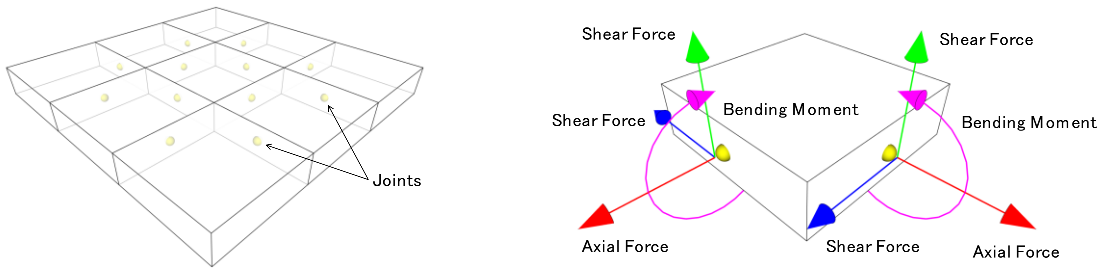

(a) Ice floe consisting of small elements (b) Forces considered at joints

Figure 1. Image of breakable ice element

In this method, a shape of a broken ice floe depends on a shape of an ice element. We used elements with a square shape in this paper. Although this results in a simple failure pattern, the movement and hydrodynamic force on the broken ice floe can be calculated more simply than complicated shapes. Ice failure occurs if one of the following conditions is satisfied at each joint:

$$\lambda_c > \varepsilon_c = L_e T_e^2 \sigma_c \quad \text{for compression failure} \tag{1}$$

$$\lambda_s > \varepsilon_s = L_e T_e^2 \sigma_s \quad \text{for shear failure} \tag{2}$$

$$\lambda_b > \varepsilon_b = \frac{L_e T_e^2}{6} \sigma_b \quad \text{for bending failure} \tag{3}$$

where λ is the constraint force/moment, ε is the threshold, L_e is the length of the element, T_e is the thickness of the element, and σ is the ice strength. Subscripts c, s, and b denote compression, shear, and bending, respectively. We conducted a cantilever-beam test in the numerical simulation and confirmed that ice failure was properly reproduced in this model (Hasegawa et al., 2019b).

Baumgarte Stabilization Method and Elastic Modulus of Breakable Ice Element

Bullet physics engine uses parameters of the constraint force mixing (Σ) and the error reduction parameter (Γ) to permit Baumgarte stabilization method (Baumgarte, 1972) which reduces constraint error efficiently. Σ and Γ are expressed as

$$\Sigma = \frac{1}{\Delta t K + D} \tag{4}$$

$$\Gamma = \frac{\Delta t K}{\Delta t K + D} \tag{5}$$

where Δt is the timestep, K is the spring constant and D is the damping constant.

Constraint forces can be reinterpreted as those arising from the same effect as a spring-damper system (Li et al., 2018), which means that elements are connected by a spring and a damper. The value of Γ is set to 0.8 within the recommended range in Bullet. It is reported that Σ greatly contributes to the hardness of constraints (Smith, 2006). Therefore, we performed the plate deflection test in the numerical simulation and compare with the experiment data. The results are shown in Figure 2 when the sizes of an ice sheet ($L_i \times B_i \times T_i$) are 5.4 × 5.4 × 0.03 m^3 and 2.7 × 2.7 × 0.03 m^3 and the element sizes (L_e) is 0.20 m. From the results, it is found that the elastic modulus is determined by the value of Σ. In this study, we used an element size of 0.20 m with Σ of 0.016 for the ice elastic modulus of about 60 MPa which was the same value as the experimental condition (Hasegawa et al., 2019b). In addition, to investigate the effect of the elastic modulus determined by this approach on ice load, numerical simulations were conducted using an element size of 0.20 m with Σ of 10^{-10} and 0.03 for the ice elastic modulus of about 200 and 30 MPa, respectively.

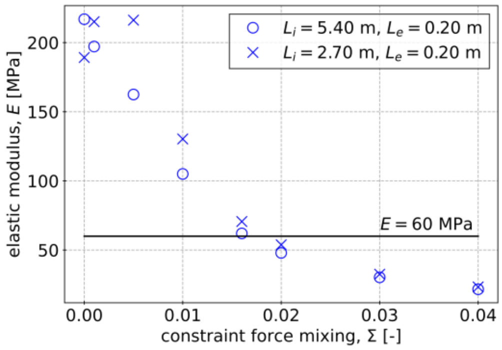

Figure 2. Influence of Σ on the elastic modulus of the numerical ice floe. The target elastic modulus (E) of 60.0 MPa is obtained from the experiment by a plate deflection method (Hasegawa et al., 2019b).

Simulation Design

We numerically simulated the structure-multiple ice floes interaction corresponding to the experiments. Table 1 summarizes the simulation conditions. The bending strength was obtained from the strength tests in the experiment. The compressive strength and the shear strength were set to be four times and twice as large as the bending strength respectively (Schwarz and Weeks, 1977). An ice-ice friction coefficient of 0.3 and an ice-structure friction coefficient of 0.2 were chosen based on values of 0.02-0.7, which are reported in the literature (Frederking and Baker, 2002; Lishman et al., 2009; Pritchard et al., 2012). Although the friction coefficient tends to increase as the sliding speed and the normal force are reduced according to Repetto-Llamazares et al. (2011) and Sukhorukov and Løset (2013), the constant value was used in our simulation. The authors have already addressed the relationship between constant friction coefficients and the behavior of numerical ice floes (Hasegawa et al., 2019b).

The coordinate system and the initial arrangement of ice floes are shown in Figure 3. The structure model has an inverted conical shape with the principal dimensions shown in Figure 4 and Table 2. The initial arrangements of ice floes were reproduced from those of the experiment (Hasegawa et al., 2019b). As an example, Figure 5 shows snapshots of the numerical simulation for the ice floe with the elastic modulus of 60 MPa. The numerical model of the structure advanced at a constant speed of 0.07 m/s from x = 2 m in the surge direction and collided with ice floes arranged in the range of $x \geq 6$ m and $-2.4 \leq z \leq 2.4$ m. No other than the surge movement of the structure model was taken into account, and the ice floes were able to move in 6 degrees of freedom. In the present simulation, the hydrodynamic force was applied to ice floes on the assumption of a simple flow around the structure (Hasegawa et al., 2018).

Table 1. Simulation conditions

	Parameter	Symbol	Unit	Value
General	timestep	Δt	s	0.02
	error reduction parameter	Γ	-	0.8
Ice	concentration	IC	%	75
	thickness	T_i	m	0.033
	density	ρ_i	kg/m^3	930.0
	bending strength	σ_b	kPa	36.4
	compressive strength	σ_c	kPa	145.6
	shear strength	σ_s	kPa	72.8
Ice floe	length × breadth	$L_i \times B_i$	m	0.60 × 0.60
	square element size	L_e	m	0.20
	elastic modulus	E	MPa	30, 60, 200
	constraint force mixing	Σ		0.03, 0.016, 10^{-10}
Water	density	ρ_w	kg/m^3	1000.0
Structure	speed	V	m/s	0.07
Coef. of restitution	ice-ice	e_{ii}	-	0.0
	ice-structure	e_{is}	-	0.0
Coef. of friction	ice-ice	f_{ii}	-	0.3
	ice-structure	f_{is}	-	0.2

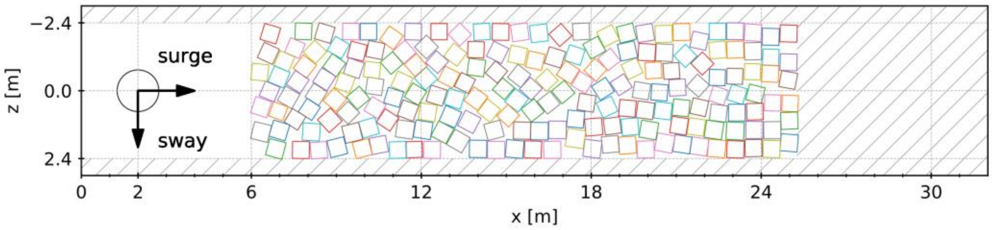

Figure 3. Initial arrangement of ice floes reproducing the experiment in the numerical simulation. The structure moved from $x = 2$ m at a constant speed in the surge direction. The shaded area shows an ice sheet placed for ice-ice contact at the wall as well as in the experiment.

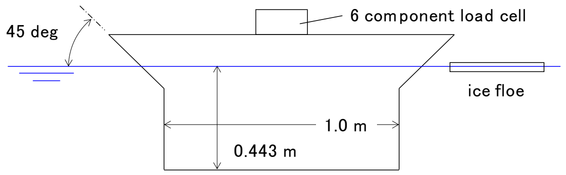

Figure 4. Cross-section view of the conical structure model

Table 2. Principal dimensions of conical structure

Parameter	Unit	Value
Breadth maximum	m	1.472
Breadth water line	m	1.228
Draft	m	0.443
Depth molded	m	0.565

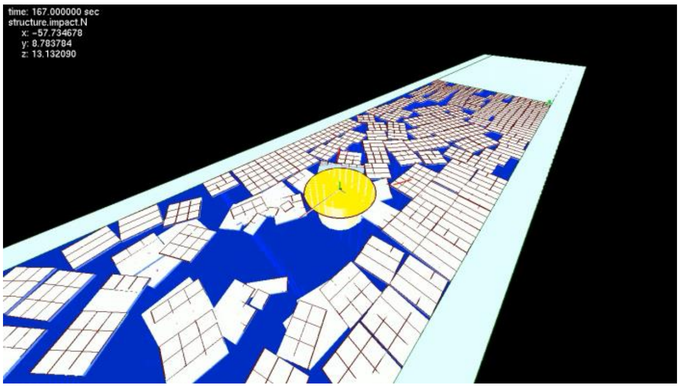

Figure 5. State of ice floes (white rectangular ones) around the structure (the yellow one) in the numerical simulation for L_e of 0.20 m. The lines (red, green, blue, and white) from the center of the structure indicate the direction (x, y, z and synthetic) and its magnitude of the ice load acting on the structure. The red and green lines from ice floes show the normal and frictional load applied to each contact point, respectively.

RESULTS AND DISCUSSIONS

In this paper, we focused on the ice load exerted on the structure in the surge direction. We defined the time at which a steady state of the load began as 0 s. Also, a hydrodynamic resistance of the structure obtained in open water was subtracted from the results. We analyzed the results of 150 s corresponding to a towing distance of 10.5 m. The mean of the maximum ice load was obtained by dividing the analysis section into three, extracting the maximum load during the 50 s, and averaging those three values. The standard deviation of the maximum ice load was calculated from the mean of the maximum ice load and the three maximum loads during each 50 s.

Figures 6 and Table 3 show the time history and the summary statistic of ice load. Figure 6 shows that peak loads had irregularities in terms of time and magnitude for each condition. From Table 3, the mean values of both simulation results with E of 30 and 200 MPa were about 10% smaller than that with E of 60 MPa. The mean of the maximum load was almost equal at about 120 N when E was 60 and 200 MPa and became minimum at about 93 N for E of 30 MPa. It is noted that repeating many simulations with different initial arrangements of ice floes may show a different trend. The mean and maximum load of the experiment for E of 60 MPa were about 38.8 N and 102.7 N, respectively (Hasegawa et al., 2019b).

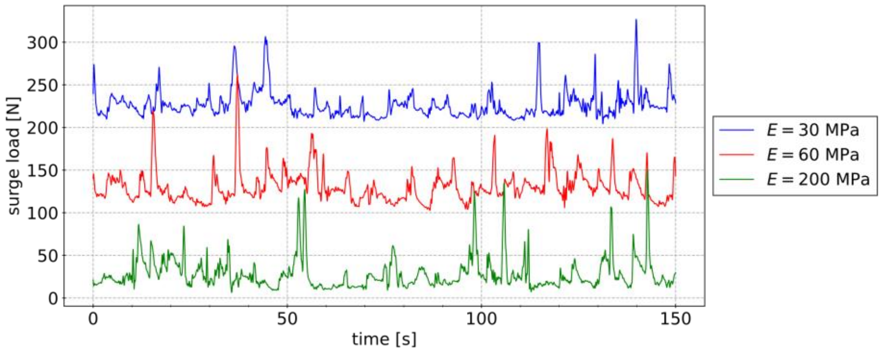

Figure 6. Ice load in surge direction in steady state. Each is shifted by 100 N.

Table 3. Summary statistics of ice load in surge direction and the ratio of the number of broken ice floes to the total number of ice floes (189) after each test. The bracketed value shows a percentage difference compared to the simulation result for E = 60 MPa.

Parameter	Mean [N]	SD [N]	Maximum [N]					Ratio of ice failure [%]
			0-50 s	50-100 s	100-150 s	Mean	SD	
E = 30 MPa	26.50 (12.5%)	15.52 (15.8%)	106.58	46.75	126.84	93.39 (20.8%)	34.00 (8.3%)	10.6
E = 60 MPa	30.28	18.43	162.22	93.10	98.50	117.94	31.39	10.1
E = 200 MPa	28.32 (6.5%)	18.67 (1.3%)	86.48	127.36	150.30	121.38 (2.9%)	26.39 (15.9%)	17.5

We summarize the ratio of the number of broken ice floes to the total number of ice floes after each test shown above in the right column of Table 3. The simulated result of the broken ice floes ratio using the same E of 60 MPa as the experiment was about a half of the experimental result of about 22% (Hasegawa et al., 2018). Although the simulated result using the lower E of 30 MPa without changing the ice strength was also about 50% less than the experimental result, the simulated result using the higher E of 200 MPa showed about a 75% increase in the number of broken ice floes in comparison with the other simulation results. It was observed that most frequent the mode of ice failure was due to bending in both the experiment and the numerical simulation.

Table 3 gives a large difference in the number of broken ice floes caused by the difference in elastic modulus even under the same ice strength conditions. We confirmed this validity with the hybrid model of ice load using Lindqvist (1989) and Kashtelijan-Poznjok-Ryblin (Nozawa, 2006. Hereafter denoted as KPR) models proposed by Uto et al. (2015).

The hybrid model is applicable for ice floes with various sizes and concentration, and areal restrictions, by coupling the limit momentum and limit stress load models. The mean of ice load is determined as the lower value from the two load scenarios, i.e., the limit momentum scenario where the load is determined by the mass and the relative speed of small ice floes, and the limit stress scenario where the load is determined by ice failure of large ice floes. Using the two load scenarios, the hybrid model of ice load (R_F) is obtained by $R_F = \min[R_{LS}, R_{LM}]$, where R_{LS} and R_{LM} are the limit stress load of the extended Lindqvist model (R_{LF}) and the limit momentum load of KPR model (R_{SF}) as follows:

$$R_{LS} = IC \times R_{LF} \qquad (6)$$

$$R_{LM} = R_{SF} \tag{7}$$

Subscripts F, LF, SF, LS, and LM denote floe, large floe, small floe, limited stress, and limited momentum, respectively. R_{LF} and R_{SF} were calculated based on Uto et al. (2015). The Lindqvist model considers the ice load as the sum of the components from ice failure by crushing and bending, and submergence of broken ice pieces. On the other hand, the KPR model assumes ice load in small ice floes as the sum of impact, dissipative, and static components. It is noted that no ice failure and submergence of ice floes are taken into account in the KPR model.

Figure 8 shows the mean ice load obtained from Equations (6) and (7) for the 0.6 m-square ice floes. R_{LM} was lower than R_{LS} when E was smaller than about 10 MPa. The limit stress load became dominant when E was larger than about 10 MPa, which means that ice failure occurs more frequently. The mean ice load of the hybrid model was about 27% larger than the experimental result of about 39 N because the Lindqvist model, which is used for larger ice floes, always includes the crushing effect which was not observed in the experiment (Hasegawa et al., 2019b). In the experiment, as shown in Figure 5, the ice floes were relatively small and ice concentration was 75%, hence the ice floes moved easily in the horizontal and vertical directions, and ice failure by crushing did not occur. Although there is a quantitative difference in the mean ice load between the simulation and the hybrid model, a qualitative change in the mean ice load due to E gives that the mean ice load decreases as E increases as shown in Figure 8. As for the managed ice condition targeted in this study, it is reasonable to consider an ice floe as an elastic body because the ice floes are plate shaped and the collision speed is small. As E increases, the characteristic length of ice floes increases, and the failure resistance due to bending decreases, so that ice failure by bending mode occurs much more frequently. Therefore, it can be explained that the simulated result for the ice floes with E of 200 MPa indicates the smaller mean ice load and the larger number of broken ice floes (see Table 3) compared to that with E of 60 MPa. The mean ice load of the hybrid model with E of 30 MPa was larger than that with E of 60 MPa, whereas the simulated result showed the opposite tendency as given in Table 3. Considering that R_{LM} is overestimated since the KPR model does not take submergence of ice floes into account, the red line of R_{LM} in Figure 8 goes down and the intersection with the R_{LS} moves towards larger E. This effect probably reduces the simulated result with E of 30 MPa.

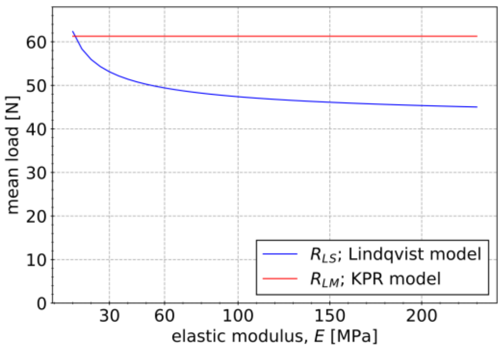

Figure 8. Mean ice load as a function of an elastic modulus of ice floes using the hybrid model proposed by Uto et al. (2015). The lower value between R_{LS} and R_{LM} is determined as the mean ice load for each elastic modulus of ice floes.

For ice floes having various characteristics such as size and strength, it is inappropriate to evaluate if ice failure will occur using the hybrid model because KPR model assumes the distribution of homogeneous ice floes. On the basis of the analytical results of an ice floe size effect on the ice failure mode by Lu et al. (2016), Sawamura and Pedersen (2018) adopted an algorithm whereby ice failure due to splitting and bending mode is considered when an ice floe size is larger than the characteristic length in their numerical simulation for an icebreaker advancing into ice-covered waters. Therefore, in our simulation model, it seems appropriate to introduce the breakable ice element into ice floes larger than the characteristic length. The characteristic length of ice floes used in this study had approximately 0.38 m when E was 60 MPa. Since the ice failure due to bending mode is related to the characteristic length of ice floes, the breakable ice element size (L_e) should be smaller than it.

CONCLUSIONS

This paper has presented the results of three-dimensional non-smooth discrete element simulations for a structure-multiple ice floes interaction under managed ice conditions. To represent ice failure, we introduced a breakable ice element consisting of small square rigid bodies with a fixed joint function of the physics engine of Bullet to our simulation model. The following results were obtained:

An elastic modulus of an ice floe can be determined by the element size and the constraint force mixing (Σ) used in Baumgarte stabilization method. Based on the hybrid model using Lindqvist and KPR models, it can be explained that the simulated result for the ice floes with E of 200 MPa indicates the smaller mean ice load and the larger number of broken ice floes (see Table 3) compared to that with E of 60 MPa. Therefore, our approach enables the non-smooth DEM simulation on global ice load by managed ice floes considering the elastic modulus.

ACKNOWLEDGEMENTS

This work was supported by JSPS KAKENHI Grant Number JP17K14890.

REFERENCES

Baumgarte, J., 1972. Stabilization of constraints and integrals of motion in dynamical systems. *Computer Methods in Applied Mechanics and Engineering*, 1(1), pp.1-16.

Catto, E., 2005. Iterative Dynamics with Temporal Coherence. *Game Developer Conference*.

Coumans, E., 2017. Bullet Physics Library version 2.86. [Online] Available at: http://bulletphysics.org/ [Accessed 1 December 2017].

Cundall, P.A., & Strack, O.D.L., 1979. A discrete numerical model for granular assemblies. *Geotechnique*, 29(1), pp.47-65.

Frederking, R., & Barker, A., 2002. Friction of sea ice on various construction materials. *Proceedings of the 16th IAHR International Symposium on Ice*, vol. 1, pp.442-449.

Gautier, D.L., & Moore, T.E., 2017. Introduction to the 2008 Circum-Arctic Resource Appraisal (CARA) Professional Paper. *The 2008 Circum-Arctic Resource Appraisal: U.S. Geological Survey Professional Paper*, 1824, 9p.

Hamano, T., Onosato, M., & Tanaka, F., 2016. Performance Comparison of Physics Engines to Accelerate House-Collapsing Simulations. *Proceedings of the IEEE International Symposium on Safety, Security and Rescue Robotics*, pp.358-363.

Hasegawa, K., Uto, S., Shimoda, H., Wako, D., & Matsuzawa, T., 2018. Numerical and Experimental Investigations of Managed Ice Loads acting on Fixed Conical Structure. *Proceedings of the 28th International Ocean and Polar Engineering Conference*, pp.1672-1678.

Hasegawa, K., Uto, S., Shimoda, H., Wako, D., & Matsuzawa, T., 2019a. Influence of Initial Arrangement of Ice Floes on Ice Loads in Non-smooth Discrete Element Method Simulation. *Proceedings of the 34th International Symposium on Okhotsk Sea and Polar Oceans*, pp.126-129.

Hasegawa, K., Uto, S., Shimoda, H., Wako, D., & Matsuzawa, T., 2019b. Non-smooth DEM Simulation for Interaction of Conical Structure and Managed Ice Floes using Breakable Ice Element. *Proceedings of the 25th International Conference on Port and Ocean Engineering under Arctic Conditions*.

Jean, M., 1999. The non-smooth contact dynamics method. *Computer Methods in Applied Mechanics and Engineering*, 177, pp.235-257.

Konno, A., Nakane, A., & Kanamori, S., 2013. VALIDATION OF NUMERICAL ESTIMATION OF BRASH ICE CHANNEL RESISTANCE WITH MODEL TEST. *Proceedings of the 22nd International Conference on Port and Ocean Engineering under Arctic Conditions*.

Li, X., Andrews, S., Jones, B., & Bargteil, A., 2018. Energized Rigid Body Fracture. *Proceedings of the ACM on Computer Graphics and Interactive Techniques*, 9.

Lindqvist, G., 1989. A Straightforward Method for Calculation of Ice Resistance of Ships. *Proceedings of the 10th International Conference on Port and Ocean Engineering under Arctic Conditions*, pp.722-735.

Lishman, B., Sammonds, P., Feltham, D., & Wilchinsky, A., 2009. The rate- and state- dependence of sea ice friction. *Proceedings of the 20th International Conference on Port and Ocean Engineering under Arctic Conditions*, POAC 09 (electronic publication).

Lu, W., Lubbad, R., Løset, S., & Kashafutdinov, M., 2016. Fracture of an ice floe: Local out-of-plane flexural failures versus global in-plane splitting failure. *Cold Regions Science and Technology*, 123, pp.1-13.

Lubbad, R., & Løset, S., 2015. Time Domain Analysis of Floe Ice Interactions with Floating Structures. *Proceedings of the Arctic Technology Conference*.

Nozawa, K., 2006. Ice Engineering (in Japanese). Seizando-Shoten Publising Co., Ltd., pp.206-213.

Polojärvi, A., Tuhkuri, J., & Korkalo, O., 2012. Comparison and analysis of experimental and virtual laboratory scale punch through tests. *Cold Regions Science and Technology*, 81, pp.11-25.

Pritchard, R.S., Knoke, G.S., & Echert, D.C., 2012. Sliding friction of sea ice blocks. *Cold Regions Science and Technology*, 76-77, pp.8-16.

Repetto-Llamazares, A. H.V., Høyland K.V., & Kim, E., 2011. Experimental studies on shear failure of freeze-bonds in saline ice: Part II: Ice-Ice friction after failure and failure energy. *Cold Regions Science and Technology*, 65, pp.298-307.

Sawamura, J., & Pedersen, E., 2018. 2D Simulation of the Icebreaking Pattern for Sea Ice Management. *Proceedings of the 28th International Ocean and Polar Engineering Conference*, pp.1672-1678.

Schwarz, J., & Weeks, W.F., 1977. ENGINEERING PROPERTIES OF SEA ICE. *Journal of Glaciology*, 19(81), pp.499-531.

Smith, R., 2006. Open Dynamics Engine v0.5 User Guide. [Online] Available at: http://ode.org/ode-latest-userguide.html [Accessed 1 December 2018].

Sukhorukov, S., & Løset S., 2013. Friction of sea ice on sea ice. *Cold Regions Science and Technology*, 94, pp.1-12.

Uto, S., Shimoda, H., Wako, D., & Matsuzawa, T., 2015. NSR Transit Simulations by Vessel Performance Simulator "VESTA" Part 2 Simple Resistance Formula of Ships in Floe Ice. *Proceedings of the 23rd International Conference on Port and Ocean Engineering under Arctic Conditions*.

Walter, O., & Kostack, K., 2015. Bullet Constraints Builder for collapse simulation. [Online] Available at: https://www.blender.org/conference/2015/presentations/190 [Accessed 1 December 2018].